Mathematical Modelling of Hydraulic Fracturing and Related Problems

Sergey V. Golovin

Lavrentyev Institute of hydrodynamics, Novosibirsk, Russia

SkolTech Energy Colloquium, March 22, 2016

Stages of the hydraulic fracturing modeling

- Fracture propagation
  - interaction of fracturing fluid with the elastic reservoir
  - fluid leak-off and interaction with pore fluid
  - rock toughness, confining stresses, etc.
- Fluid flow
  - fluid-proppant mutual influence
  - proppant transport, settlement
  - bridging of proppant
- Fractured well production
  - production forecast
  - multiple wells interaction

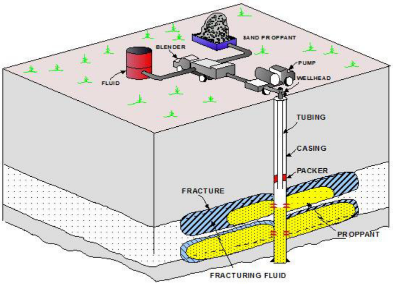

- Hydraulic fracture control
  - Determination of the size and location of the fracture

Fracture growth in a poroelastic medium

Khristianovich-Geertsma-de-Klerk (KGD)[1]

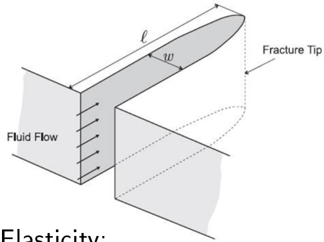

Flow in the fracture:

Mass balance: $\dfrac{\partial w}{\partial t} + \dfrac{\partial Q}{\partial x} = -q_L$

Carter's formula: $q_L = \dfrac{2C_L}{\sqrt{t - t_{\exp}(x)}}$

Poiseuille's formula: $Q = -\dfrac{w^3}{12\mu}\dfrac{\partial p}{\partial x}$

Elasticity:

$$w(t,x) = \frac{4}{\pi E'} \int_0^l \big(p(t,\xi) - \sigma\big) B(x,\xi) d\xi, \quad E' = \frac{E}{1-\nu^2}, \qquad (1)$$

where E and ν are the Young's modulus and Poisson's ratio,

$$B(x,\xi) = \ln \left| \frac{\sqrt{l^2 - x^2} + \sqrt{l^2 - \xi^2}}{\sqrt{l^2 - x^2} - \sqrt{l^2 - \xi^2}} \right|. \qquad (2)$$

[1] S.V. Golovin, V.I. Isaev, A.N. Baikin, D.S. Kuznetsov, A.E. Mamontov. (2015) Hydraulic fracture numerical model free of explicit tip tracking // Int. J. Rock. Mech. Min. Sci. 76 174-181.

Perkins-Kern-Nordgren (PKN)

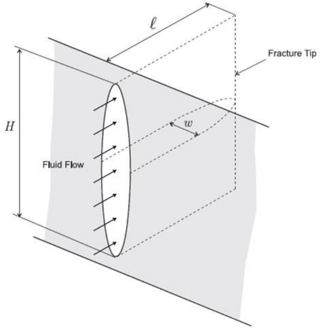

Flow in the fracture:

Mass balance: $\dfrac{\partial A}{\partial t} + \dfrac{\partial Q}{\partial x} = -Hq_L,$

Carter's formula: $q_L = \dfrac{2C_L}{\sqrt{t - t_{\text{exp}}(x)}}$

Poiseuille's formula:

$$Q = -\frac{\pi E'}{512\mu}\frac{\partial w_{\max}}{\partial x}$$

Elasticity:

$$w(t,z) = \frac{4\big(p(t)-\sigma\big)}{E'}\sqrt{\frac{H^2}{4} - z^2}, \quad A = \frac{1}{4}\pi H w_{\max}$$

State of the Art

Mostly used hydraulic fracturing models:

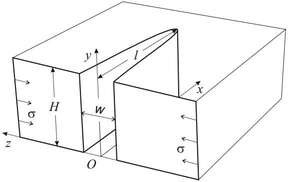

- KGD, PKN, penny-shaped models (Classic)
- P3D, Planar3D
- 3D models

Some drawbacks:

- Influence of pore pressure to the strain is not properly accounted
- Leak-off requires additional assumptions (a subject of discussions)
- Infinite fluid pressure at the fracture tip

Review of modern results:

- J. Adachi, E. Siebrits, A. Peirce, J. Desroches, (2007) *Computer simulation of hydraulic fractures*. Int. J. Rock. Mech. & Mining Sci. 44 739–357.
- E. Detournay, (2016) *Mechanics of Hydraulic Fractures*. Ann. Rev. Fluid Mech. 48(1):311-339

Fracture in a poroelastic medium[2]

Biot's equations of poroelastisity

$$\operatorname{div}\tau = 0, \quad \tau = \underbrace{\lambda \operatorname{tr} E(\vec{u})\,\mathrm{I} + 2\mu E(\vec{u})}_{\text{Elastic Stress}} - \underbrace{\alpha p\,\mathrm{I}}_{\text{Pore Pressure}}$$

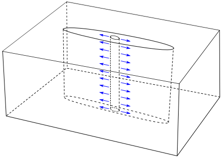

$$S_e \frac{\partial p}{\partial t} = \operatorname{div}\left(\frac{k_r}{\eta_r}\nabla p - \alpha\frac{\partial \vec{u}}{\partial t}\right)$$

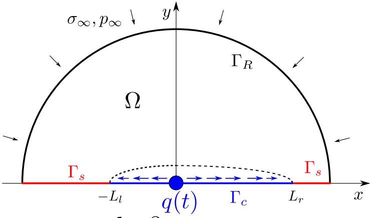

$$q_l = -\frac{k_r}{\eta_r}\frac{\partial p}{\partial y} = -\kappa(p - U)$$

$$\mathbf{\Gamma_R} : p = p_\infty, \quad \tau\langle\vec{n}\rangle = -\sigma_\infty\,\vec{n}$$

$$\mathbf{\Gamma_s} : u_y = 0, \quad v = 0, \quad p_y = 0$$

$$\mathbf{\Gamma_c} : \tau\langle\vec{n}\rangle = -U\,\vec{n}$$

$$\mathbf{\Gamma_c} : \frac{\partial v}{\partial t} = \frac{\partial}{\partial x}\left(\frac{v^3}{3\eta_r}\frac{\partial U}{\partial x}\right) - q_l;$$

$$\pm\frac{v^3}{3\eta_r}\frac{\partial U}{\partial x}\Big|_{y=0,x=0\mp} = \frac{q(t)}{2} = \frac{Q(t)}{2H}$$

[2] V.V. Shelukhin, V.A. Baikov, S.V. Golovin, A. Ya. Davletbaev, V.N. Starovoitov, (2014). Fractured water injection wells: Pressure transient analysis // Int. J. Sol. & Struct., 51(11), 2116-2122.

Non-Stationary Self-Similar Solution[3]

The representation of solution:

$$
\begin{cases}
u(t,x,y) = t^{1/6}\,U(\xi,\eta) \\
v(t,x,y) = t^{1/6}\,V(\xi,\eta) \\
p(t,x,y) = t^{-1/3}\,P(\xi,\eta)
\end{cases}
\quad\Bigg|\quad
\begin{aligned}
&\xi(t,x,y) = \frac{x}{\sqrt{t}} \\
&\eta(t,x,y) = \frac{y}{\sqrt{t}} \\
&L_i(t) = \gamma_i\sqrt{t}, \quad i = r,l
\end{aligned}
$$

Assumptions:

- Injected **flow rate:** $q = q_0\,\mathbf{t}^{-1/3}$
- **Velocity** of fracture tips: $v_{tip} = v_0\,\mathbf{t}^{-1/2}$.

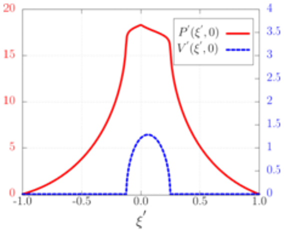

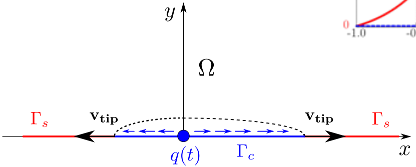

[3] S.V. Golovin, A.N. Baykin, (2015). Stationary dipole at the fracture tip in a poroelastic medium // Int. J. Sol. & Struct., 69–70, 305–310

Solution Method: Fracture Growth Criterion

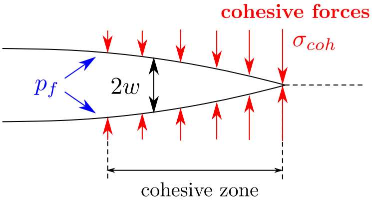

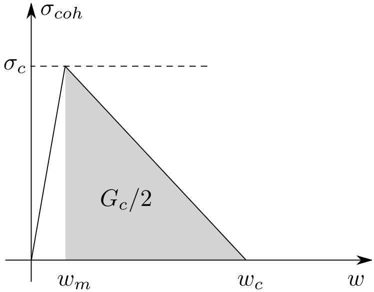

Case studies: Common parameters

Parameter	Value
Young's Modulus, E	17 GPa
Poisson's Ratio, ν	0.2
Reservoir Permeability, k_r	100 mD
Biot Coefficient, α	0.75
Storativity, S_e	1.5×10^{-8} Pa^{-1}
Closure Stress, σ_∞	3.7 MPa
Reservoir Pressure, p_∞	0 MPa
Reservoir Fluid Viscosity, η_r	10^{-3} Pa $\cdot$ sec
Fracture Fluid Viscosity, η_f	10^{-3} Pa $\cdot$ sec
Rate per Unit Height, q	10^{-2} m^2/sec

Case Studies: Pressure and fracture aperture

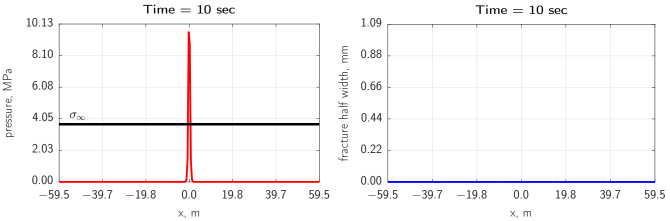

Pressure and **half-width** over the boundary $y = 0$

Case Study: Non-Uniform Closure Stress

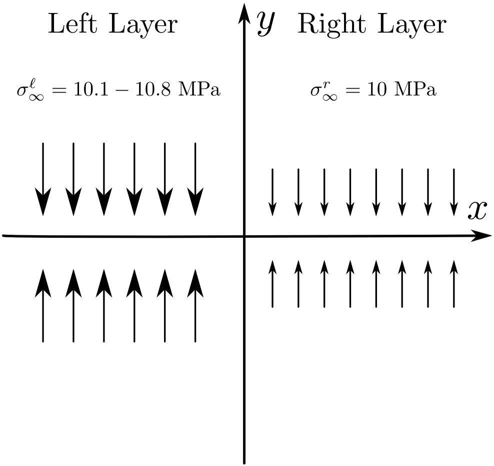

Case Study: Non-Uniform Closure Stress

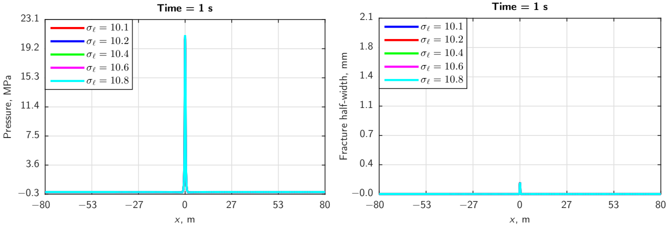

Pressure and fracture aperture over the boundary $y = 0$.

Case Studies: Non-Uniform Permeability

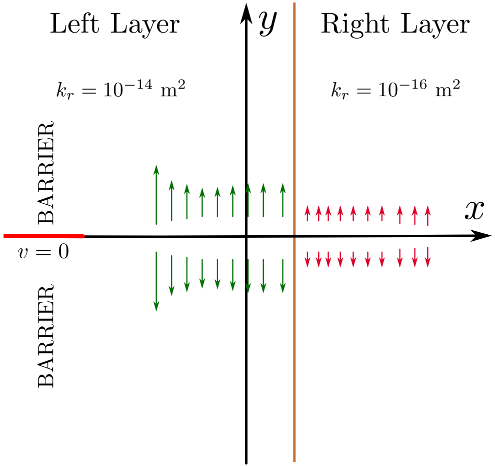

Case Studies: Non-Uniform Permeability

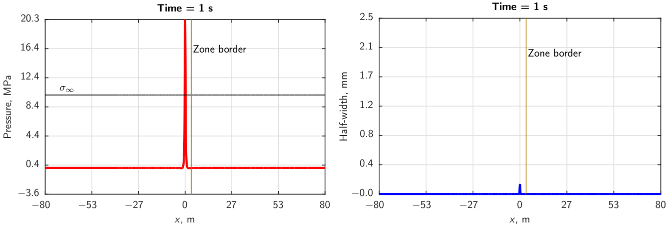

Pressure and fracture aperture over the boundary $y = 0$.

Case Studies: Non-Uniform Permeability

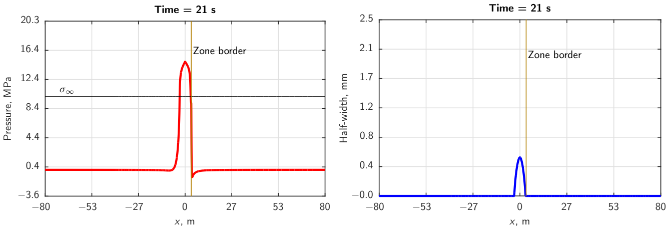

Pressure and fracture aperture over the boundary $y = 0$.

Case Studies: Non-Uniform Permeability

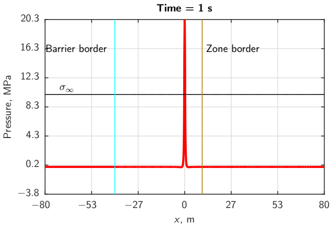

Pressure and fracture aperture over the boundary $y = 0$.

Case Studies: Non-Uniform Permeability

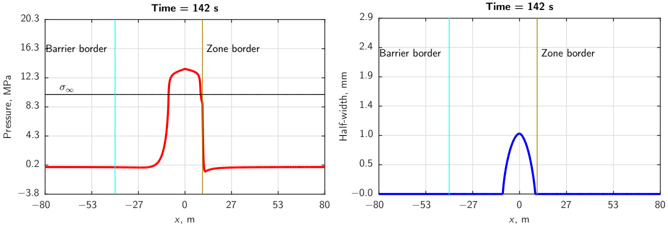

Pressure and fracture aperture over the boundary $y = 0$.

Case Studies: Non-Uniform Permeability

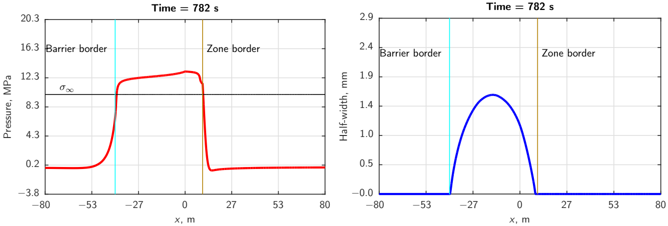

Pressure and fracture aperture over the boundary $y = 0$.

Inhomogeneity of fracturing fluid

Statement of the problem

- The fracture design supposes a stage of pumping of increasing concentration of proppant
- Model of the fracture growth should take into account
  - Non-uniform distribution of proppant in a crack
  - Instabilities due to different viscosities of fluid components
  - Mutual influence of proppant distribution and fracture opening

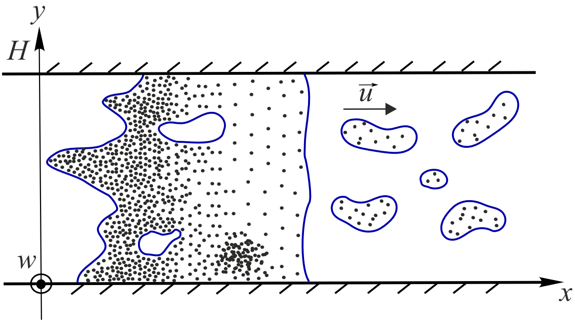

Pseudo two-speed model

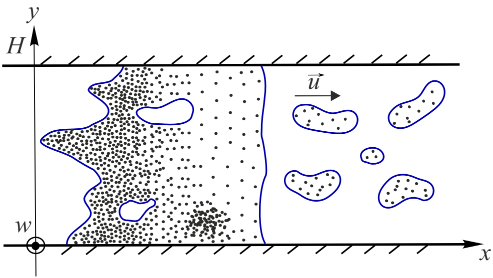

Mass conservation laws:

$$\begin{cases} \dfrac{\partial(\rho w)}{\partial t} + \nabla \cdot \left(\rho w \vec{u}\right) = -Q_{lf}, \\ \dfrac{\partial}{\partial t}(wd) + \nabla \cdot (wd\vec{u}) = 0 \end{cases}$$

$$u = cu_p + (1-c)u_f, \quad s = \overline{d} \equiv \frac{1}{cH}\int\limits_{\Gamma_p} d\, dy.$$

Pseudo two-speed model

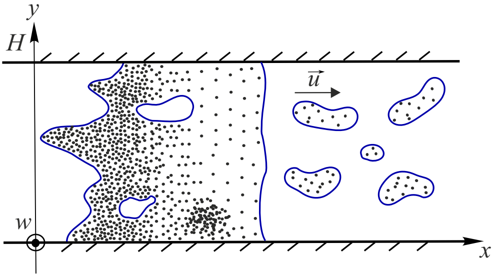

Averaged system:

$$\begin{cases} \dfrac{\partial(cw)}{\partial t} + \dfrac{\partial(cwu_p)}{\partial x} = -v_l c \left(1 - \dfrac{s}{s_l}\right) + \mathcal{Q}, \\ \dfrac{\partial w}{\partial t} + \dfrac{\partial(wu)}{\partial x} = -v_l \left(1 - \dfrac{cs}{s_l}\right), \\ \dfrac{\partial s}{\partial t} + u_p \dfrac{\partial s}{\partial x} = \dfrac{s}{w} \left(v_l \left(1 - \dfrac{s}{s_l}\right) - \dfrac{\mathcal{Q}}{c}\right). \end{cases}$$

Micro-polar and visco-plastic fluids [4]

Examples of micro-polar and visco-plastic fluids: fracturing fluid with proppant, drilling fluid, blood, etc.

In the model we take into account fluid-particle and particle-particle interaction: $\mathbf{v}$ is the suspension velocity, $\boldsymbol{\omega}$ is the angular speed of micro-rotations, p is the pressure, $B = \nabla \mathbf{v} + \epsilon \cdot \boldsymbol{\omega}$ is the strain tensor. The stress tensor is

$$T = -pI + 2\mu_1 B_s + 2\mu_2 B_a + \tau_* \frac{B}{|B|}, \quad \text{if} \quad B \neq 0$$

Right: dimensionless flow rate vs. dimensionless pressure gradient. The curves from top to bottom correspond to increase of viscosity μ_2. The top curve $\tau_* = \mu_2 = 0$ is the Navier-Stokes.

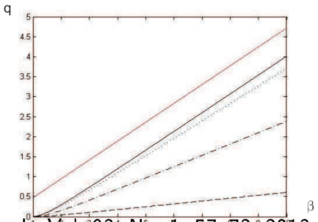

[4] Shelukhin V. Ruzicka M. // Z. Angew. Math. Mech. Vol. 93, No. 1, 57–72. 2013

Inflow to a horizontal multiply-fractured well

Inflow to a horizontal multiply-fractured well

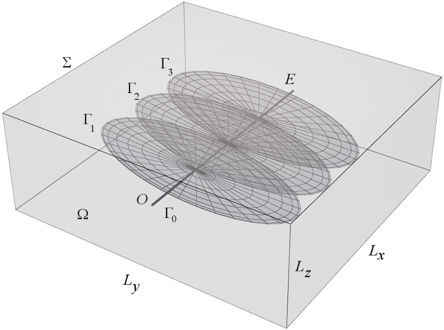

Physical parameters:

p — pressure

$\rho = \text{const}$ — dencity

$m = m(p)$ — porosity

ε — elastic capacity

$k = k(x, y, z)$ — rock permeability

μ — fluid viscosity

Proposed 2D-model accounts for

- Arbitrary net of fractures with different conductivities of segments
- Variable in space and time physical parameters of the reservoir
- Arbitrary boundary conditions over the outer boundary an at the borehole (given pressure or flow rate)

Optimization of fractures geometry

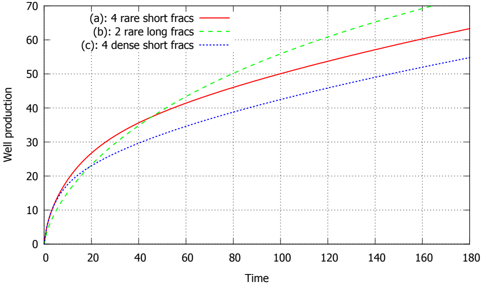

Well production (10^3 m^3) versus time (days): (a) — four short rare fractures; (b) — two long fractures; (c) — four dense short fractures

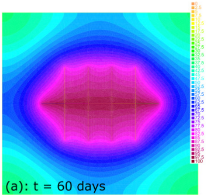

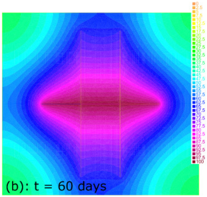

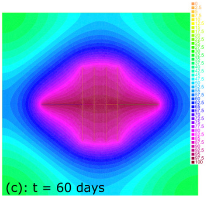

Pressure distribution at $t = 60$ days.

An "arbitrary" fracture net

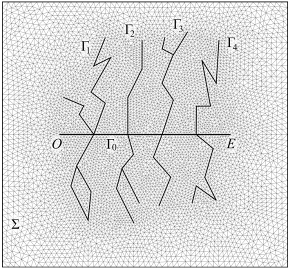

An "arbitrary" set of fractures and the computational mesh

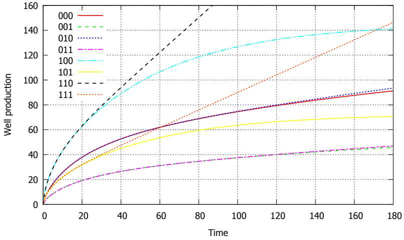

Well production (10^3 m^3) versus time (days).

An “arbitrary” fracture net

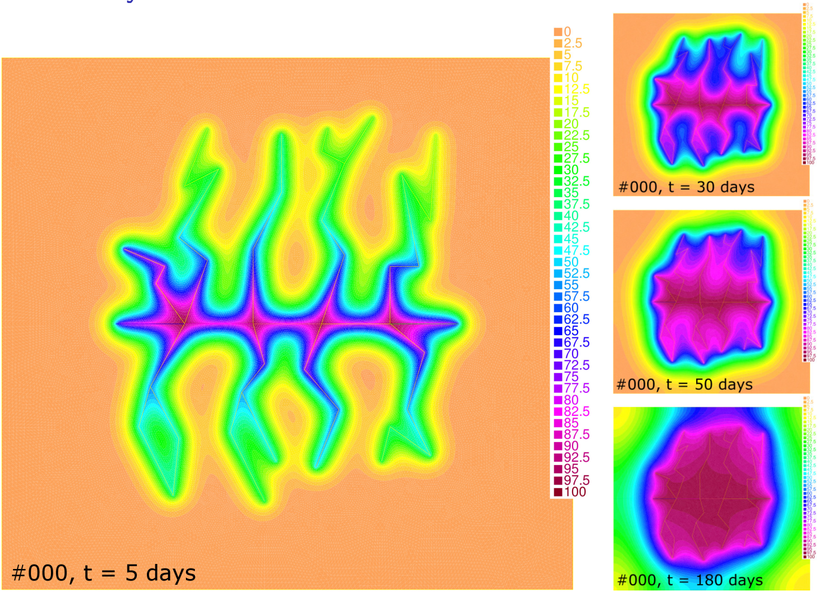

Pressure distribution: $k = 1$ mD, $p|_O = 100$ atm, given pressure over outer boundary

Hydraulic fracture control

Phase shift between waves of velocity and pressure

By the directi numerical modelling it is shown that under non-stationary injection/suction of fluid into the fractured well, the phase shift between the velocity v and pressure p is observed.

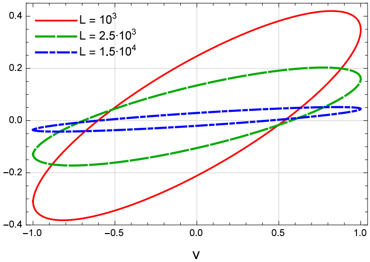

vp – diagrams for different fracture lengths L

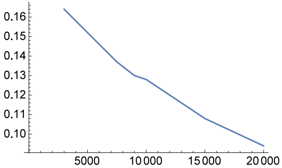

Phase shift vs. L

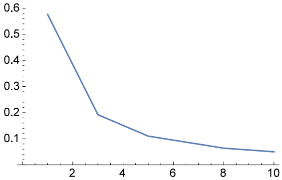

Phase shift vs. ω

This observation allows determination of L by the solution of the parametric optimization problem.

Hydraulic fracture and Maxwell-Wagner polarisation [5]

After the pumping stop, the fracture is closing.
1 is an invasion zone, 2 virgin zone, φ is the streaming potential, σ is the conductivity of filtrating electrolytes:

$$\mathbf{Q} = -\lambda_{11}\nabla p - \lambda_{12}\nabla\varphi, \ \mathbf{J} = -\lambda_{21}\nabla p - \lambda_{22}\nabla\varphi,$$

$$\lambda_{11} = k/\eta, \quad \lambda_{22} = \sigma, \quad \lambda_{12} = F\sqrt{\lambda_{11}\lambda_{22}}$$

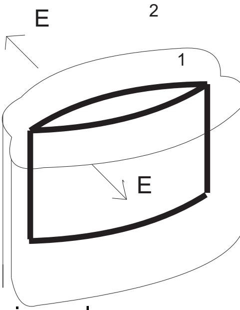

Electrokinetic coefficients λ_{ij} are discontinuous on the invasion front.Electric field E is perpendicular to the hydraulic fracture and growths as the rations $\lambda_{11}^{(2)}/\lambda_{11}^{(1)}$ и $\lambda_{22}^{(1)}/\lambda_{22}^{(2)}$ decrease. This corresponds to decrease of viscosity and electric conductivity of invading fluid.

[5] Eltsov I.N., Moshkin N.P., Shelukhin V.V., Epov M.I. // Doklady Physics, 2016, V. 467, № 2.

Related problems: cerebral haemodynamics

Cerebral arteriovenous malformations [6]

An arteriovenous malformation is a tangle of arteries and veins that affects normal cerebral blood circulation.

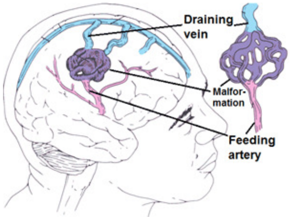

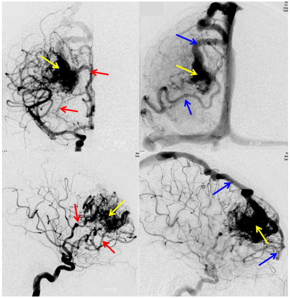

In the brain, damage occurs through 4 mechanisms:

- Theft of blood to neighbouring nerve tissue.
- Brain haemorrhage.
- Compression of surrounding nervous tissue.
- Making the flow of cerebrospinal fluid (CSF) more difficult

[6] Pictures source: http://www.neuros.net

Cerebral arteriovenous malformations [6]

Embolisation of arteriovenous malformation.

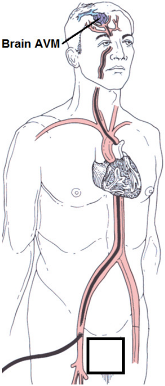

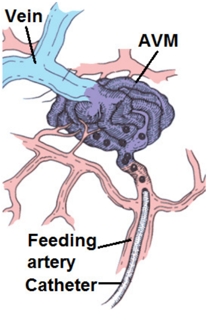

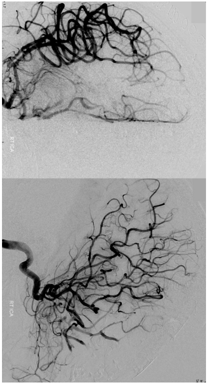

[6] Pictures source: http://www.neuros.net

Experimental data

In vivo measurements of pressure and velocity in brain vessels were done in Meshalkin Research Institute Of Blood Circulation Pathology [7]

Volcano ComboMap

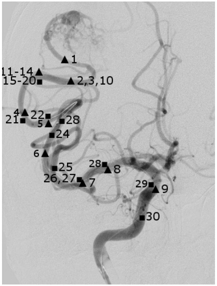

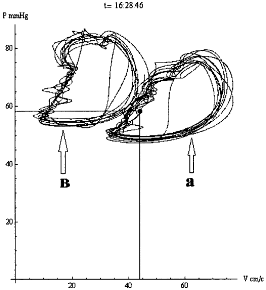

VP-diagram in the afferent of AVM

A – before the embolisation,

B – after the embolisation.

[7] A. P. Chupakhin, A. A. Cherevko, A. K. Khe, et. al. Measurement and analysis of cerebral hemodynamic parameters in the presence of brain vascular anomalies // Circulation Pathology and Cardiac Surgery. 2012, No. 4, pp. 27–31.

Experimental data

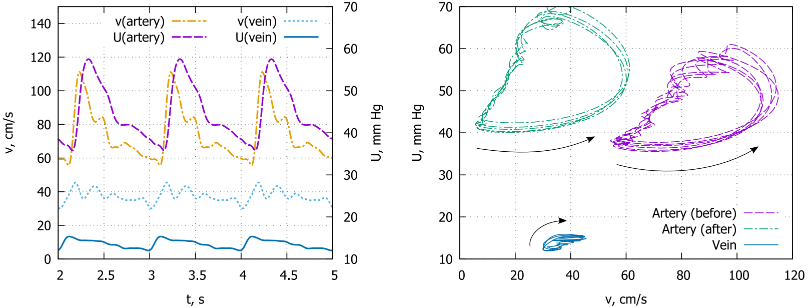

Typical graphs of *in vivo* measured velocity and pressure of the blood flow in a feeding artery (afferent) and a draining vein of an AVM.
Left: Time series.
Right: vp-diagram in the afferent of the AVM before and after the embolisation, and in the draining vein.

Numerical experiments

Length scale	$L = 10$ cm	Vessel radius	$R = 0.1$ cm
Porosity	$m_0 = 0.2$	Fluid viscosity	$\mu = 2.4 \cdot 10^{-2}$ g/(cm s)
Permeability	$k = 2 \cdot 10^{-9}$ cm^2	Elastic capacity	$\varepsilon = 3.75 \cdot 10^{-7}$ cm s^2/g
Time	$T = 1$ s	Walls permeability	$\kappa = 10^{-4}$ cm^2 s/g

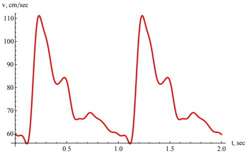

Input velocity $v(O)$

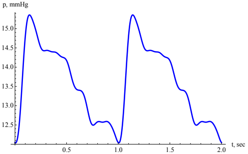

Output pressure $p(E)$

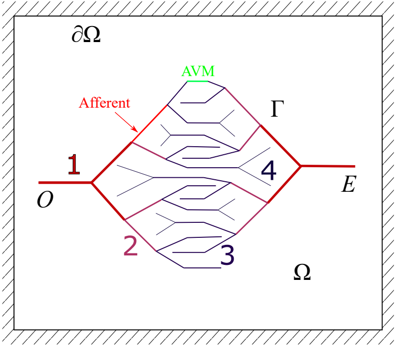

Arterial (left) and venous (right) trees of vessels

Numerical results

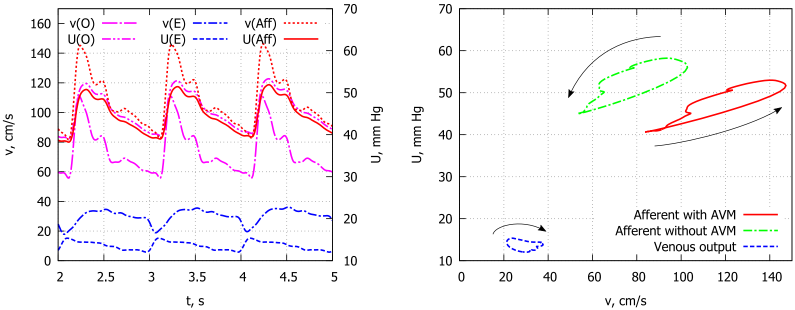

Computational results for velocity and pressure.
Left: Time series at the roots of the arterial (O) and the venous (E) trees, and in the afferent.
Right: vp-diagram in the afferent and at the root E of the venous tree before and after the embolisation.

Further development

- Modelling of 3D fractures in inhomogeneous reservoir;
- Interpretation of the mini-frac tests;
- Estimation of the fracture conductivity after the pressure drop;
- Dynamics of multi-fracturing;
- Filtration of multiphase fluids and interaction with HF;
- Dynamics of non-Newtonian fluids in tubes and fractures;

THANK YOU FOR ATTENTION!